AIAA AVIATION Forum
June 15-19, 2020, VIRTUAL EVENT
AIAA AVIATION 2020 FORUM

10.2514/6.2020-3217

Aspects of analysis and simulation of a flaperon ditching scenario

Argiris Kamoulakos[1]
MH370-CAPTIO Team Member, Paris, France (akamoulakos@yahoo.com)

In the wake of the disappearance of the MH370 Boeing 777 and the recovery of the right wing flaperon debris, a ditching scenario has been envisaged by the investigating authorities. In this respect, this paper attempts to assess the forces exerted by fluid-structure interaction upon a guided-ditching flaperon both through analytical and numerical means and compare the results with the evidence. The author presents a modified version of the Karman wedge water impact theory, suitably adapted for a single flat panel ditching case, which leads to a simple analytical relation for the total hydrodynamic force as a function of the flaperon horizontal and vertical speeds and its angle of impact. Validation of the analytically obtained force to that obtained by Smoothed Particle Hydrodynamics (SPH) water simulations is presented. An extension of the analytical relation is made for the flaperon section failure stresses as a function of velocity vector and angle of impact with the perspective towards areas containing fastened parts. A basic Finite Element Model (FEM) of the flaperon is then conceived from available geometric and material data and subjected to a typical ditching impact. The type and place of failure of the flaperon (notably its trailing edge) appears in accordance with the analytically obtained upper bounds and with the state of the recovered flaperon.

I. Nomenclature

α	=	angle of inclination of the under-surfaces with the horizontal (angle of deadrise)
σ_{av}	=	average principal membrane stress of the flaperon skin due to hydrodynamic bending effect
σ_{max}	=	maximal membrane stress of the flaperon skin around a fastener stress concentration
C_{α}	=	pressure coefficient due to trailing edge end-effects
C_{3D}	=	pressure coefficient due to lateral end-effects
C_{σ}	=	stress concentration coefficient around fastener holes
c	=	flaperon chord length
d	=	moment arm distance of force to spar section where fracture happened
F_v	=	vertical component of the resultant pressure force acting on the body
F_n	=	resultant pressure force acting normal to the wetted surface
F_m	=	flaperon skin membrane force due to hydrodynamic bending effect
l	=	length of the body
m	=	mass per unit length of the body
M	=	total mass of the body
n_{ply}	=	number of composite fabric plies comprising the skin of the flaperon
t_{ply}	=	thickness of each plie of the flaperon skin
V_0	=	initial vertical (impact) speed of the body
V	=	instantaneous vertical speed of the body
V_{x0}	=	prescribed horizontal ditching speed
V_{y0}	=	prescribed vertical ditching speed
V_n	=	equivalent ditching speed normal to the instantaneous water surface
w	=	width of the flaperon spar where fracture happened

[1] Scientific Director, ESI Group, 3 bis rue Saarinen, 94528 Rungis, FRANCE.

x = half width of the wedge at the plane of the undisturbed water surface
x_{eff} = effective half width of the wedge for added mass estimation
y = depth of immersion normal to the plane of the undisturbed water surface

II. Introduction

"On 07 March 2014 at 1642 UTC a Malaysia Airlines (MAS) Flight MH370, a Beijing-bound international scheduled passenger flight, departed from Runway 32R, KL International Airport [KLIA] with a total of 239 persons on board (227 passengers and 12 crew). The aircraft was a Boeing 777-200ER, registered as 9M-MRO." (extract from the Malaysian accident investigation report).

A little bit later that day the aircraft vanished from the radars. Ever since, its whereabouts remain a mystery.

In the years that followed, a very limited amount of debris has been recovered in the Indian ocean coastal lines of Africa, Mauritius and Isle de Reunion. From this debris, only three pieces have been formally identified as definitely belonging to that aircraft: the right flaperon, the right inner flap and the trailing edge of the left outer flap.

Despite extensive search, no traces of the aircraft itself have been found and the case is (at least for now) closed after the final accident investigation reports from Malaysian authorities in 2018.

Many scenarios have been proposed regarding what happened to this aircraft.

The CAPTIO team has put forward a coherent account of the possible trajectory the aircraft would had followed, that satisfies as much as possible the available satellite and Air Traffic Control data, and it leads to a potential ditching close to the Christmas Islands. The details of this work can be found in the CAPTIO website http://mh370-captio.net/.

The recovered confirmed debris of this flight holds the key to the aircraft final moments. In particular, the flaperon debris which has been extensively examined by the Direction Générale de l' Armement (DGA) Ministry of Defense in France [1] and is pictured in Fig. 1, at the moment it was transferred for investigation.

Fig. 1 Flaperon being recovered by the French authorities at Ile de La Réunion.

What is very intriguing is the missing part of the trailing edge (highlighted by CAPTIO in Fig. 1). The conclusion of the French report was that a ditching process was the most probable cause. The author who is a member of the CAPTIO team embarked to complement the DGA study by attempting to examine (as much as possible with the available data) the validity of the ditching assumption from a theoretical and a numerical (simulation) point of view.

In this process he revisited the Von Karman theory for water impact and adapted it / extended it accordingly.

III. Strategy for modelling ditching through numerical simulation

Ditching involves fluid-structure interaction with large topology changes of the fluid as a consequence of the creation of waves during the penetration by the structure. One practical way to simulate ditching is to model the fluid with a particles method in order to allow large topological changes and mixing, that is, phenomena that are very difficult to be captured by traditional numerical methods, like the Finite Element method (FE) for instance. The particles method that was used to model the fluid (water) was the Smoothed Particle Hydrodynamics method (SPH). See Fig. 2 below for basic concepts.

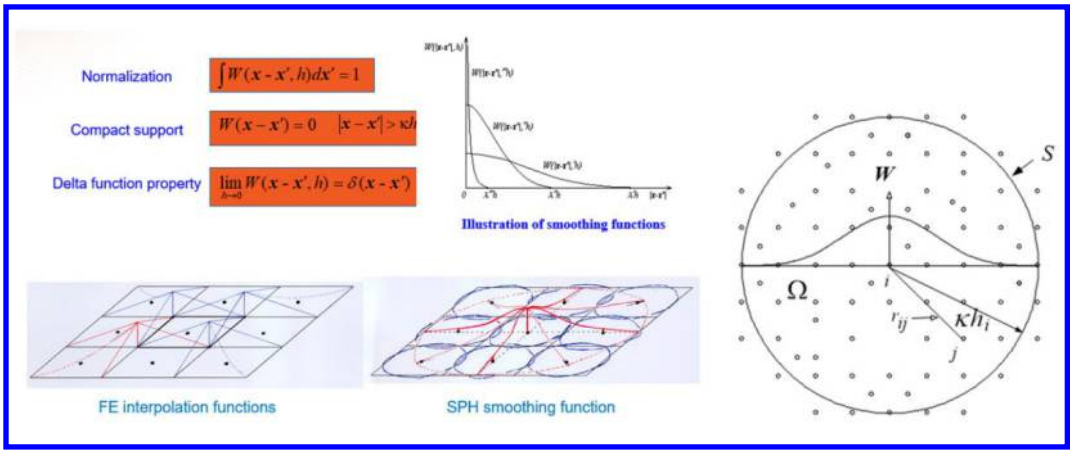

Fig. 2 Foundation of SPH idealizations as compared to FE

In order to choose the appropriate discretization of the fluid domain for ditching, a systematic investigation of the Von Karman wedge benchmark was done. The problem setup is as in Fig. 3 below corresponding to an infinitely long horizontal cylindrical body with a wedge-shaped undersurface impacting vertically a semi-infinite fluid domain.

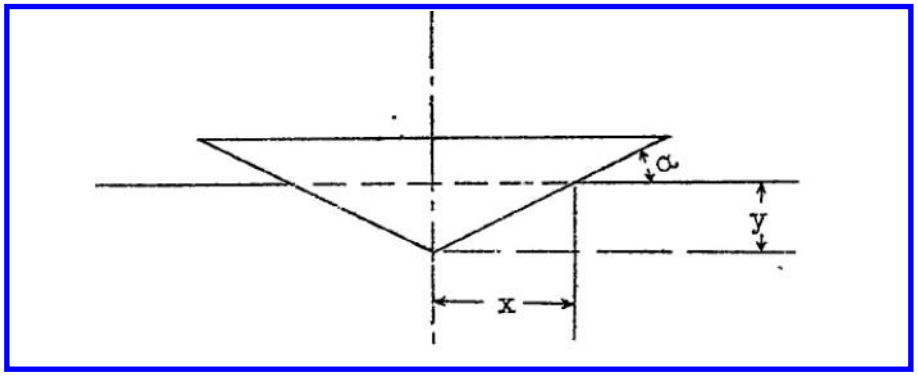

Fig. 3 Definition of the Von Karman wedge from [3]

The problem is essentially 2D as the third dimension that goes to infinity is self-similar, hence the problem corresponds to the class of "plane strain" problems.

The simulations were done using the explicit transient dynamic code VPS (PAMCRASH) of ESI Group [9] and using the 2D and 3D options for SPH modelling, as required. The material model for the water requires an appropriate Equation Of State (EOS). Although traditionally a polynomial EOS is used for water under impact, since in ditching (under the velocities we are interested) the water compressibility is very small, it is more efficient to adopt the Murnahan-Tait EOS [2,9].

Before proceeding with the simulations, the necessary theoretical foundation is presented below and the VPS-based simulations are used to validate and complement this foundation.

IV. Basic Von Karman theory for water impact of seaplane floats

Von Karman [3] examined the problem of an infinitely long horizontal perfectly rigid prismatic body with a wedge-shaped undersurface as it strikes vertically an infinitely long horizontal undisturbed surface of water in order to calculate analytically an estimate of the force per unit length acting between the body and the water at "first impact" stages. In his pioneering approach, he ignored the subsequent hydrodynamic flow effects, the viscosity or cavitation effects, any horizontal relative velocity to the sea and finally the "Archimedes" force (buoyancy), as he was interested at the "first impact" scenario.

In this sense the problem is tackled from a "conservation of momentum" approach between the before impact and after impact state of the system, without any gravitational effects and in 2D.

Let m be the mass per unit length of the body (seaplane), α the angle of inclination of each of the wedge undersurfaces with the horizontal and y the vertical distance the body travels in time from the initial point of impact with the water (depth of immersion). The time varying motion of the body within the water will provoke a disturbance in a mass of water beneath it, which will provide inertial resistance to the penetration. This is the "virtual mass". Von Karman, using the 2D assumption, estimated the virtual mass to be equal to the mass of water contained in a semi-cylinder of diameter equal to the width of the wedge at the plane of the undisturbed (original) water surface.

The semi-cylindrical assumption for the virtual mass comes from the fact that a flat plate in 2D, fully immersed in a fluid and accelerating through it, experiences theoretically an added inertia from a mass of fluid that is contained within a circular cylinder of diameter equal to the width of the plate. The rear part of the plate experiences a suction force from the rear semi-cylinder of water while the front part a compression force from the forward semi-cylinder of water. In our case we have half the domain filled with air and half with water, hence only the semi-cylinder of water represents any added inertial force.

The conservation of momentum at any time t during the penetration then gives:

$$mV_0 = mV + \frac{1}{2}\pi x^2 \rho V \tag{1}$$

where ρ is the water density and V_0 the initial vertical speed. Setting the following for the instantaneous velocity:

$$V = \frac{dy}{dt} = \tan\alpha \cdot \frac{dx}{dt} \tag{2}$$

and using the following identity:

$$\frac{d^2x}{dt^2} = \frac{d}{dx}\left[\frac{1}{2}\left(\frac{dx}{dt}\right)^2\right] \tag{3}$$

we can substitute Eq. (2) in Eq. (1) and using Eq. (3) we can obtain for a body with an out-of-plane length l and total mass M, the instantaneous retardation as below:

$$\frac{d^2y}{dt^2} = \frac{{V_0}^2 \cot\alpha}{M\left(1+\frac{\rho l\pi x^2}{2M}\right)^3}\rho l\pi x \tag{4}$$

The associated vertical force F_v can then be obtained from Newton's law as:

$$F_v = M\frac{d^2y}{dt^2} = \frac{{V_0}^2 \cot\alpha}{\left(1+\frac{\rho l\pi x^2}{2M}\right)^3}\rho l\pi x \tag{5}$$

The case we are interested in this paper is for a constant prescribed immersion speed V_0 of the wedged body and this can be obtained if we assume that the total mass of the body is infinite. In this case Eq. (5) becomes:

$$F_v = {V_0}^2 \rho l\pi x \cot\alpha \tag{6}$$

A. The Wagner correction and its modification by the author

Wagner [4] examined the same problem by trying to take account of the wave generated by the body during its immersion in the water. Since the water displaced by the immersing body rises along its sides, the width of the wetted surface and the associated mass of the flow should be greater than those based on the flat width in the plane of the undisturbed surface, as Von Karman assumed.

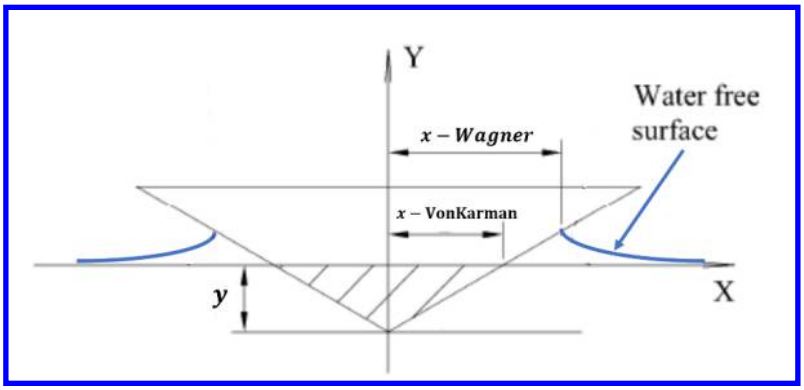

Fig. 4 Definition of the Wagner "correction"

Assuming that the water particles at the top of the water upflow move vertically up (see Fig. 4) and in accordance to the analytical 2D velocity profile for the water crest at the interface with an inclined flat plate being immersed in a horizontal water surface, he determined the "effective" width of the wedge at the tip of the wetted surface. He discovered that for a triangular cross section, which is the case for the wedged shape undersurface of Von Karman, that it is 1.57 (or $\frac{\pi}{2}$) times larger of that by Von Karman.

This is sometimes termed as the "Wagner correction", although it is not sure that Wagner was aware of Von Karman's work as his approach was independent and different.

Wagner proceeded to re-estimate the "virtual mass" of the fluid based on this risen wetted surface and this was consequently estimated as $\left(\frac{\pi}{2}\right)^2$ of that by Von Karman. This implied also that the resultant vertical force would be scaled by $\left(\frac{\pi}{2}\right)^2$ as compared to that of Von Karman.

However, over the years it became evident that while Von Karman's formula in equations Eq. 4, Eq. 5 and Eq. 6 underestimated the resultant vertical force during immersion, the Wagner correction produced a force that greatly overestimated this force as compared to experimental measurements.

Researchers like Mayo [5] gave a great account of the differences between the Von Karman and Wagner theory and all the efforts done to reconcile them, and all actually came down to a large effect to the definition of the added mass.

The author believes that Von Karman's estimation for the added mass appears to have a good theoretical foundation as a first guess, since at that time the means at his disposal were very limited. However, Wagner's extension of basing the added mass on a cylinder whose radius is the "effective" width of the wedge at the tip of the wetted surface, appears not justifiable, as the fluid near the tip of the wetted surface is already part of the "spray" and is already moving tangentially, thus has already delivered its momentum to the wedge. Hence a cylinder thus defined will include much more fluid mass than the one that should be moving downwards with the plate.

Payne [8] is one to seriously challenge the choice of added mass size by Wagner, in favour of that of Von Karman and in the process he quotes amongst other researchers the experimental results of Bisplinghoff at MIT in the 60s. These results showed that the actual "effective" width of the wedge (excluding spray which is physically present) should be on average between 1.2 and 1.35 times larger than that of Von Karman.

In this paper we have no experimental results but we use high fidelity simulations (VPS code) for our work which include the spray and we have found that the best factor for correcting the Von Karman effective wedge width was about 1.25, and the corresponding hydrodynamic force comparisons for all cases of interest in this article were very

encouraging, as it will be shown in the rest of the paper. Since 1.25 is practically $\sqrt{\frac{\pi}{2}}$ and for the sake of similarity with the existing equations we can define the effective wedge width for added mass definition as:

$$x_{eff} = \sqrt{\frac{\pi}{2}}\, x_{VonKarman} \tag{7}$$

The consequence of the above is that the added mass now will be scaled by $\frac{\pi}{2}$ as compared to that of Von Karman and similarly the corresponding hydrodynamic force. Substituting Eq. (7) to Eq. (1) for x and repeating the derivation of the hydrodynamic force we get:

$$\boldsymbol{F_v = \frac{\pi^2}{2} V_0^{\,2} \rho l x \cot \alpha} \tag{8}$$

The above new form of the Von Karman equation is the cornerstone of this paper.

It is very challenging to visualize the added mass in ditching but one "imaginative" way through simulation can be to depict the part of the fluid that moves downwards with the body at any given instant.

A wedged object was modelled as a rigid body using the VPS code (PAMCRASH) and it impacted a stationary mass of water (modelled with SPH 2D technology as explained earlier).

The geometry of the wedge was such it makes an angle of 30 degrees with the undisturbed surface of the water and the prescribed immersion speed was 10 m/s.

Figure 5 below attempts to show the added masses based on the Von Karman (yellow), Wagner (blue) and the author (red).

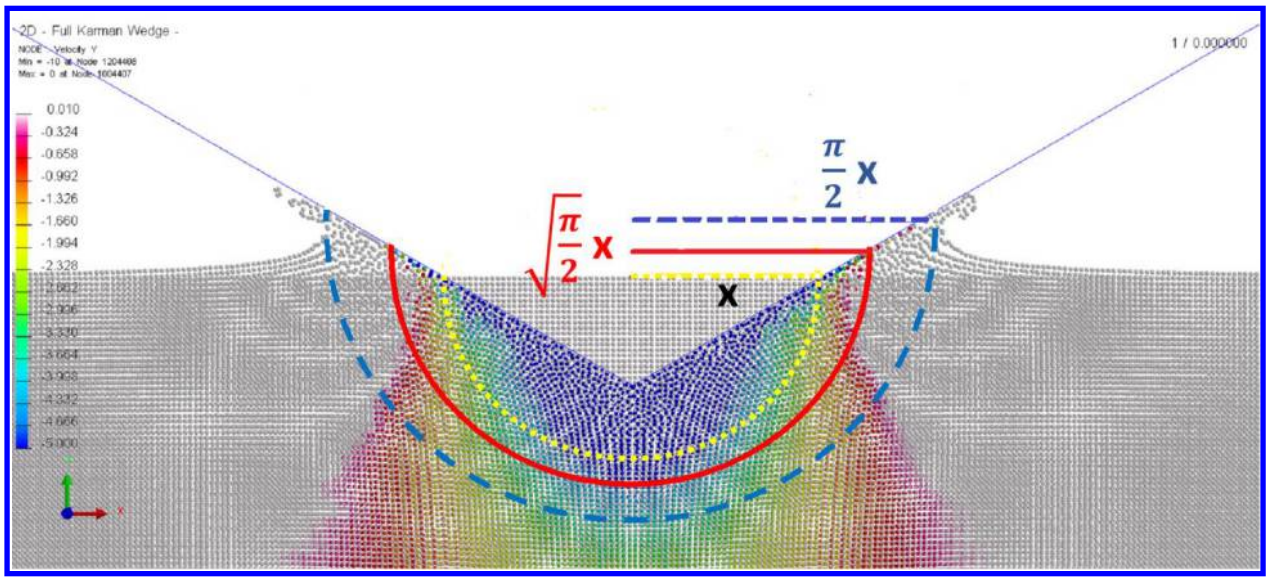

Fig. 5 Added masses according to Von Karman (yellow), Wagner (blue) and the author (red)

The initial undisturbed fluid is shown in order to allow the definition of the Von Karman added mass that uses the undisturbed surface as reference.

It can be seen that the Von Karman added mass (based on x) does not include some of the fluid that moves significantly downwards and certainly not any part from the water elevation at the crest, by definition, while the Wagner added mass (based on $\frac{\pi}{2}x$) contains a lot of fluid that is not moving downwrads or is moving within the "spray" at the crest that is not part of the added mass, as shown by Bisplinghoff.

The definition from the author (in red, based on $\sqrt{\frac{\pi}{2}}x$) extends the Von Karman added mass to include parts of the fluid still participating in the downward motion plus includes the effective width of Bisplinghoff (the part of the crest

that has contour colours showing vertical motion), hence it is a reasonable compromise and hints visually to why the results of this paper shown later on are encouraging.

V. Adaptation of the Von Karman theory to a flat plate at vertical impact

Noting that an inclined flat plate under vertical impact resembles half the Von Karman wedge, one can assume that the associated vertical force evolution during vertical immersion will basically be half the force predicted by the Von Karman wedge but adjusted by a coefficient that represents the force reduction due to the end-effects. This is to compensate for the change of flow around the lowest end of the plate which is no longer the apex of a wedge but an open end.

Hence dividing Eq. (8) by 2 we get:

$$F_v = C_\alpha \left(\frac{\pi}{2}\right)^2 V_0^{\,2} \rho l x \cot \alpha \tag{9}$$

where $C_\alpha$is a coefficient that is inclination dependent and modifies the force according to its end-effects and to any minor adjustments regarding to the choice of Eq. (7) for the effective wedge width.

This can be investigated through simulation using the same wedged object defined before, that is, having an angle of 30 degrees with the undisturbed surface of the water and a prescribed vertical immersion speed of 10 m/s.

Then the same model was modified to only half of the wedge, ie a flat plate at 30 degrees inclination.

Figures 6 and 7 show a typical snapshot of the instantaneous velocity vectors of the water flow, the difference in the flow pattern due to the end-effects at the lowest end of the plate is obvious.

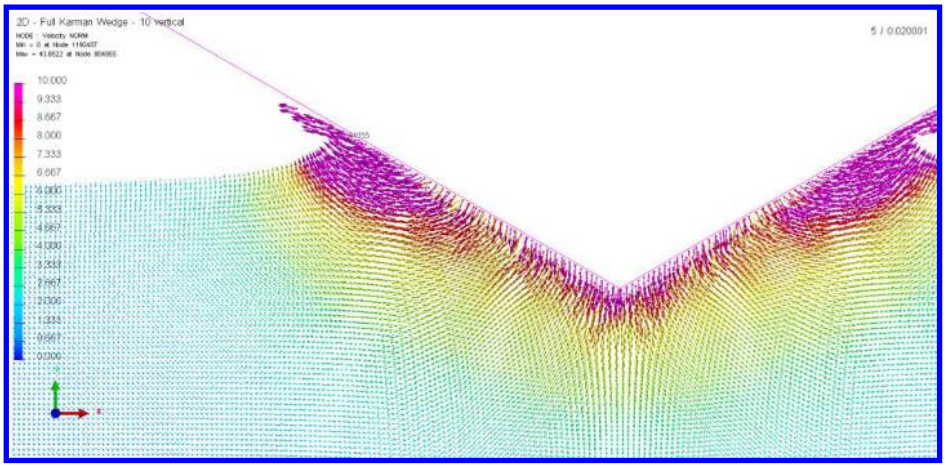

Fig. 6 Velocity vector contours for the Von Karman wedge vertical impact

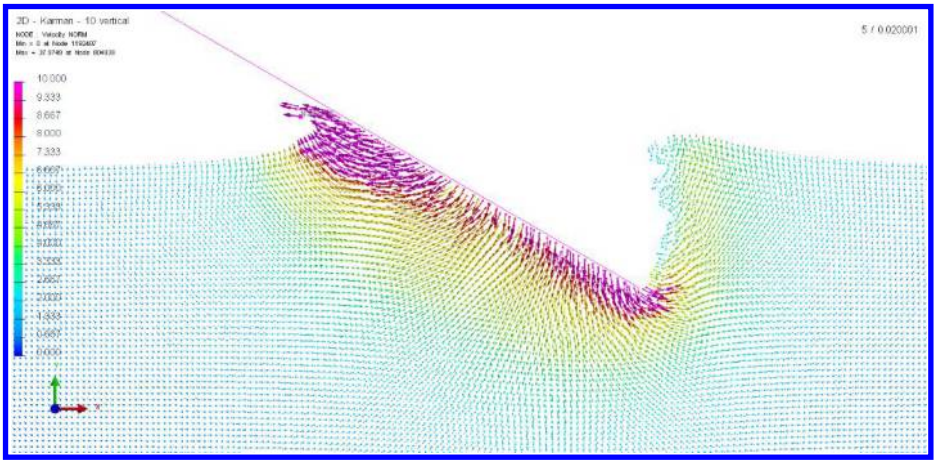

Fig. 7 Velocity vector contours for the flat plate (half Von Karman Wedge) vertical impact

The evolution of the resultant vertical force with respect to the immersion vertical displacement was extracted from the simulations for both the Von Karman wedge and the corresponding flat plate. It was also calculated according to Eq. (8) and Eq. (9) while the coefficient C_α was adjusted in Eq. (9) in order to fit as close as possible the simulation results. The comparison is as below:

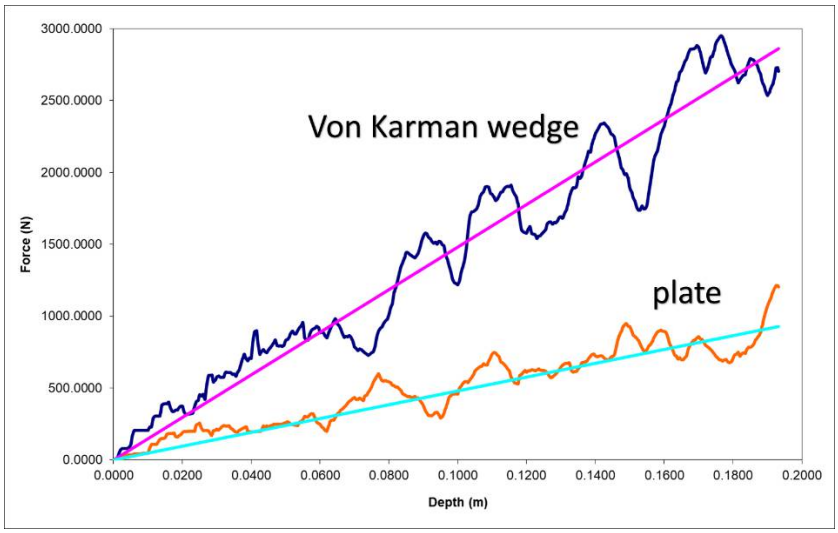

Fig. 8 Force versus immersion depth comparison between simulation and theory – 30 degrees

It can be seen that the comparison between the simulation and the theory is quite encouraging. The theoretical curve that corresponds to the plate 30 degrees case was obtained with C_α equal to $\frac{13}{20}$

The same exercise was repeated with wedges of angle 15 and 45 degrees respectively and the corresponding results are as below:

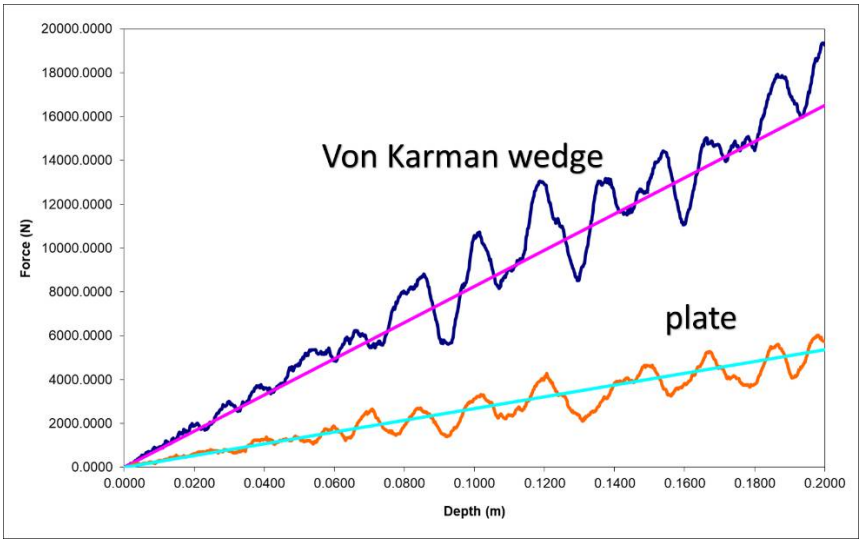

Fig. 9 Force versus immersion depth comparison between simulation and theory – 15 degrees

The theoretical curve that corresponds to the plate 15 degrees case was obtained with C_α equal to $\frac{16}{20}$

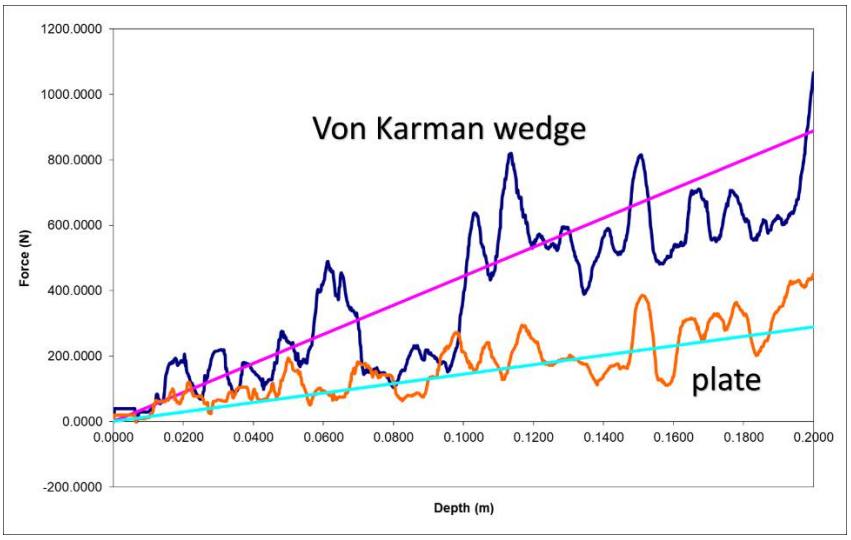

Fig. 10 Force versus immersion depth comparison between simulation and theory – 45 degrees

The theoretical curve that corresponds to the plate 45 degrees case was obtained with C_α equal to $\frac{11.5}{20}$

The above three values of the C_α , as given in Table 1, were used to define an interpolation function for intermediate values of inclination α as below:

$$C_\alpha \sim 1.3561 - 0.206 \ln \alpha_{in\ degrees} \tag{10}$$

or

Table 1 Evolution of C_α versus α

α (degrees)	C_α
15	$\frac{16}{20}$
30	$\frac{13}{20}$
45	$\frac{11.5}{20}$

VI. Adaptation of the Von Karman theory to a flat plate at inclined impact

For a vertical immersion of a wedge, it is obvious that the only velocity that matters is the vertical one and the pressure applied to the wedge surfaces during immersion has a zero resultant in the horizontal direction due to symmetry, while only the vertical force component on the two surfaces matters and it is additive.

However, this is not the case for a half wedge, ie, a flat plate, the resultant pressure from the flow field evolution will have a horizontal and vertical resultant force. Equation (9) will provide only the vertical force based on Von Karman's theory, since it was obtained from vertical momentum conservation only.

Considering what kinematics disturb the water and provide the flow around the plate one can see that it is not the vertical velocity that really matters but the effective velocity normal to the plate which will disturb the flow and provoke the associated hydrodynamic forces. Under the assumptions of this paper, any inclined plate with a velocity vector aligned along the plate surface will enter the water like an arrow and "not disturb" the water (the thickness of the plate is not a geometric parameter, only its surface, and under these conditions it is invisible to the fluid).

We can rewrite Eq. (9) with respect to the vertical distance variable y as below:

$$F_v = C_\alpha \left(\frac{\pi}{2}\right)^2 V_0^{\ 2} \rho l y (\cot \alpha)^2 \tag{11}$$

Defining the velocity component normal to the plate as:

$$V_n = V_0 \cos\alpha \tag{12}$$

and realizing that this velocity is the sum of the projections of the horizontal V_{x0} and vertical velocities V_{y0} of the plate as below:

$$V_n = V_{x0} \sin a + V_{y0} \cos\alpha \tag{13}$$

we can rewrite Eq. (11) in the following form:

$$\boldsymbol{F_v = C_\alpha \left(\frac{\pi}{2}\right)^2 \left(V_{x0} + V_{yo} \cot\alpha\right)^2 \rho l y} \tag{14}$$

Equation (14) gives us an estimate of the vertical force evolution on an inclined flat plate under steady inclined immersion due to steady horizontal and vertical speeds of V_{x0} and V_{yo} respectively.

The simulation model of the flat plate inclined at 30 degrees was used to validate Eq. (14) for inclined impact.

For a constant horizontal velocity V_{x0} of 55 m/s and a constant vertical speed V_{y0} of 20 m/s the vertical force evolution from the simulation results is presented against the above theory, using equation (10) for the variation of C_α.

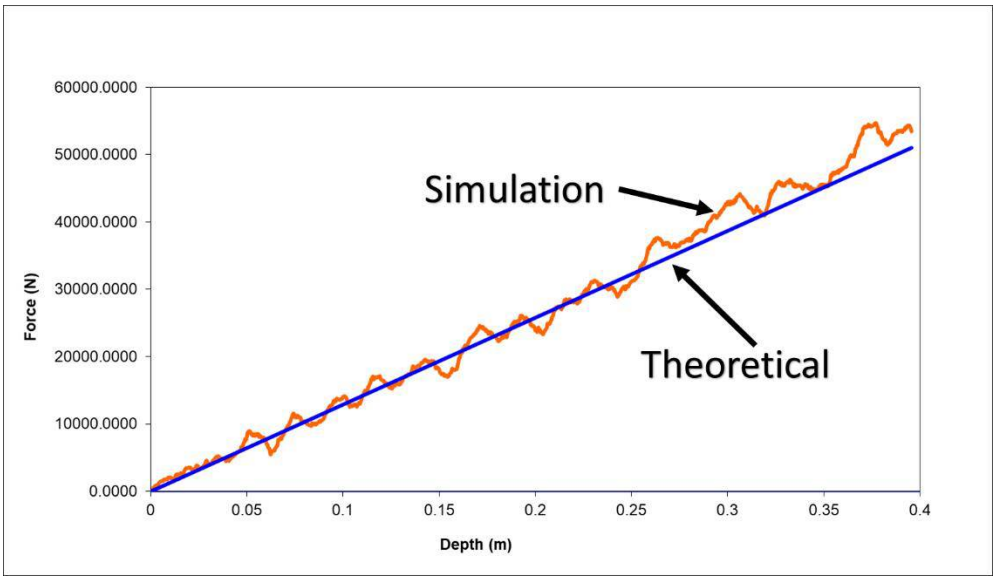

Fig. 11 Force versus immersion depth for 55 m/s horizontal – 20 m/s vertical speeds

We can see from Fig. 11 that the comparison is quite favorable. This validates the assumption that the effective normal speed with respect to the water mass is a major physical variable in ditching or planing, which is of course no surprise as the stagnation streamline is normal to the plate surface.

A typical guided ditching scenario with a constant 68.42 m/sec (153 miles/hour) horizontal speed and 2.54 m/sec (500 ft/min) vertical speed and with the SPH discretization in 2D plain strain chosen in the previous section is shown during a typical instant in the simulation as in Fig. 12.

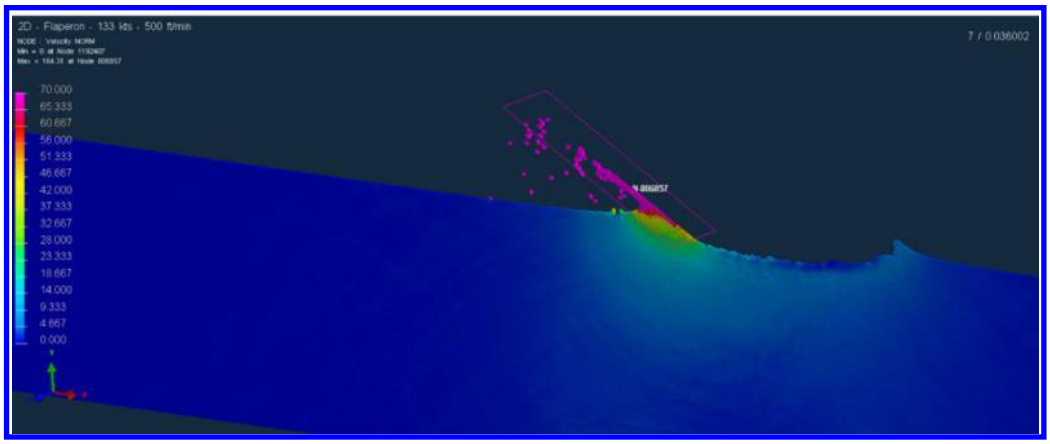

Fig. 12 Velocity contours of 2D SPH ditching simulation of plate at 30 degrees

A wide range of speed combinations were simulated as shown below, and the different vertical force evolution curves we obtained. Important observations can be made once we indicate the equivalent normal speed V_n that corresponds to these combinations and the equivalent vertical immersion speed for a Von Karman scenario on a flat plate V_0 as calculated from Eq. (12), shown in Table 2.

Table 2 Equivalence between inclined ditching and vertical immersion

V_{x0} (m/s)	V_{y0} (m/s)	V_n (m/s)	V_0 (m/s)
55	10	36.16	41.76
55	20	44.82	51.75
50	30	50.98	58.87
68.42	2.54	36.41	42.04
68.42	5.08	38.61	44.58
70	20	52.32	60.41

The flat plate was **simulated** for an inclined immersion with a combination of horizontal and vertical speeds of 55m/s - 10m/s and then by the "equivalent" vertical immersion with a Von Karman speed of 41.76 m/s and the results are shown in Fig. 13.

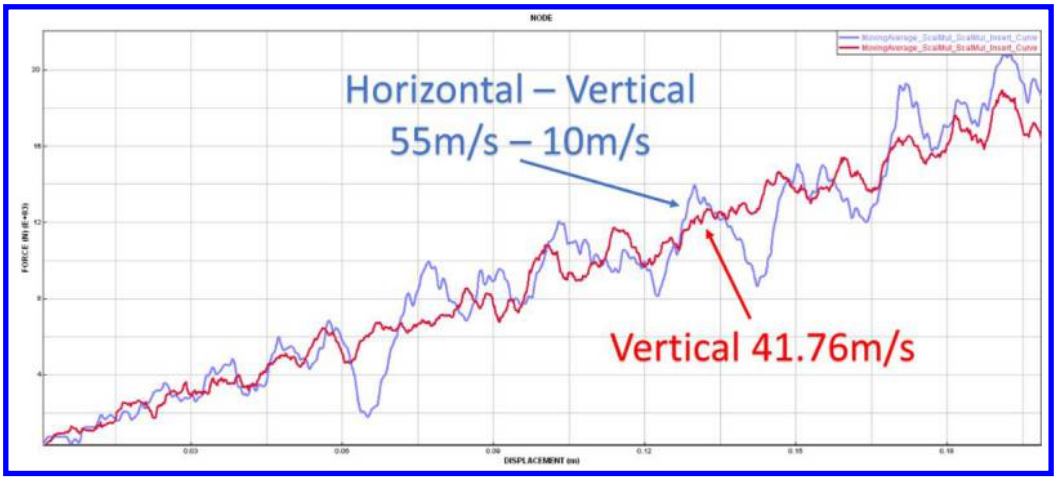

Fig. 13 Resultant vertical force versus depth of immersion evolution / Equivalence between inclined and vertical ditching

It can been that the resultant vertical force evolution in the two cases is practically identical validating the fact that there is an equivalence between vertical slamming and inclined ditching, that is, for every combination of horizontal and vertical speeds in inclined water impact there is an equivalent vertical impact speed that produces the same force evolution.

This validates also the theoretical approach for adapting the Von Karman theory to the inclined impact cases.

Furthermore it can be seen, for instance, that the combinations of 50 m/s – 30 m/s and 70 m/s – 20 m/s results in similar V_n and hence expected similar hydrodynamic force evolution and similar damage on the flaperon for the same α is expected.

More importantly the same can be said for the combinations 68.42 m/s – 2.54 m/s (controlled ditching approach, shown in Fig. 12) and 55 m/s – 10 m/s (uncontrolled ditching approach).

That is, the horizontal – vertical speed combination, is not an obvious differentiator for deciding if the flaperon would be damaged or not, but instead it is its corresponding normal speed relative to the water surface at a particular sea state.

VII. Flaperon skin stresses during ditching

Switching the terminology from flat plate to flaperon (as we assume that the lower surface of the flaperon resembles a flat plate), we want to estimate an upper bound of the skin stresses during ditching for any spanwise section along its chord.

Assuming a flaperon of chord c and inclined by angle α, we seek to evaluate the stresses σ of the upper and lower skin in bending at a spar section passing through the point S located at a distance c_s from the leading edge.

What is of interest is the magnitude of the total hydrodynamic force. Since viscous effects are neglected (no boundary layer) there is no tangential force possibly exerted by the fluid upon the plate but only a normal force and the vertical force of Eq. (14) is simply the vertical projection of that normal force.

Hence the resultant hydrodynamic force normal to the plate F_n shall be as below:

$$F_n = \frac{F_v}{\cos\alpha} \tag{15}$$

We assume that the resultant force F_n from Eq. (15) due to the ditching under constant horizontal and vertical speeds V_{x0} and V_{yo} respectively is applied at a distance d from point S towards the trailing edge as in Fig. 14.

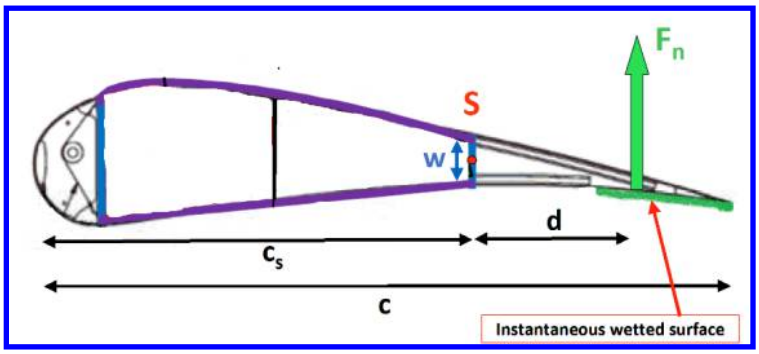

Fig. 14 Flaperon sectional definitions

Using moment equilibrium, the major part of the bending moment at point S due to the force F_n shall be equal to the sectional bending couple from the upper / lower skin compressive / tensile forces F_m through that section. Hence:

$$Bending\ Moment = F_n d = F_m w \tag{16}$$

where w is the sectional width (width of the spar at that section).

Taking into account the fact that the flaperon skin is made out of a number of composite plies we can define the average uniform principal skin stress σ_{av} as related to the skin forces like below:

$$F_m = \sigma_{av} l n_{ply} t_{ply} \tag{17}$$

where the skin is made overall from a total number of n_{ply} plies each having a thickness t_{ply}

Combining Eq. (17), Eq. (16) and Eq. (15) we can obtain the average uniform principal skin stress, whether tensile or compressive due to the bending moment induced by the hydrodynamic force F_n.

We will have to introduce a coefficient, C_{3D}, in the force calculation for the fact that the true flaperon is a finite body with strong end-effects regarding the hydrodynamic flow during ditching around its spanwise ends (pressure relief like the wing tip end-effect). This coefficient will be investigated in the next section.

In order to attempt to estimate the level of stresses that can produce skin failure, we need to take one more factor into account, the fact that the flaperon skin failed along a line of fasteners, hence the local stress concertation factor C_σ has to be somehow incorporated. This type of factor is always multiplicative as it locally scales up the stresses. In plane stress isotropic medium problems, for a circular hole under bi-axial far-field loading it is 2 while for a uniaxial far-field loading it is 3.

Finally, taking all the above into account we can have the following form for the maximal local average skin stress σ_{max} in bending:

$$\boldsymbol{\sigma_{max} = C_\alpha C_{3D} C_\sigma \left(\frac{\pi}{2}\right)^2 \left[\frac{(V_{x0}+V_{yo}\cot\alpha)^2 \rho y d}{n_{ply} t_{ply} w \cos\alpha}\right]} \quad \textbf{(18)}$$

where:

$$2 < C_\sigma < 3 \quad (19)$$

As the fastener holes we refer to are those of screws, their pre-tensioning is an extra variable, but very difficult to quantify in real life in how it affects the C_σ. This was left out of this investigation as it can always be incorporated by modifying the C_σ coefficient. Similarly for any modification to C_σ due to the proximity effect between the fasteners, as here they are treated in isolation from each other.

VIII. Simulation of the guided ditching of a flaperon as a rigid body 3D

The flaperon was modelled in 3D as a rigid body and was analyzed in a 3D ditching scenario as shown in Fig. 15 and for the same configuration in a 2D simulation.

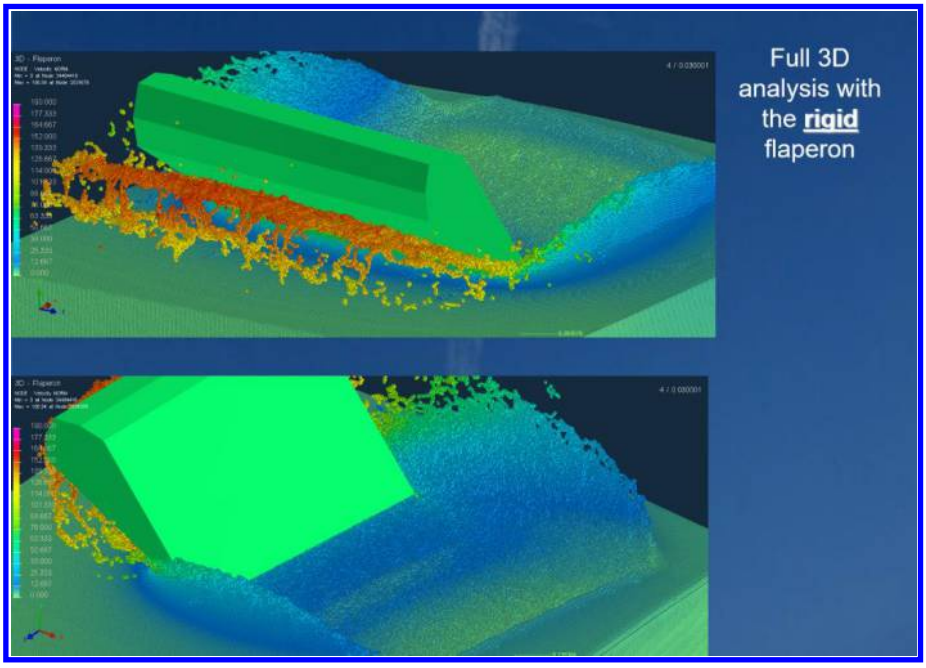

Fig. 15 SPH ditching simulation of 3D rigid flaperon

The resultant vertical force evolution was compared between the 2D and 3D simulations in order to obtain an estimate of the C_{3D} coefficient. The comparison is shown in Fig. 16.

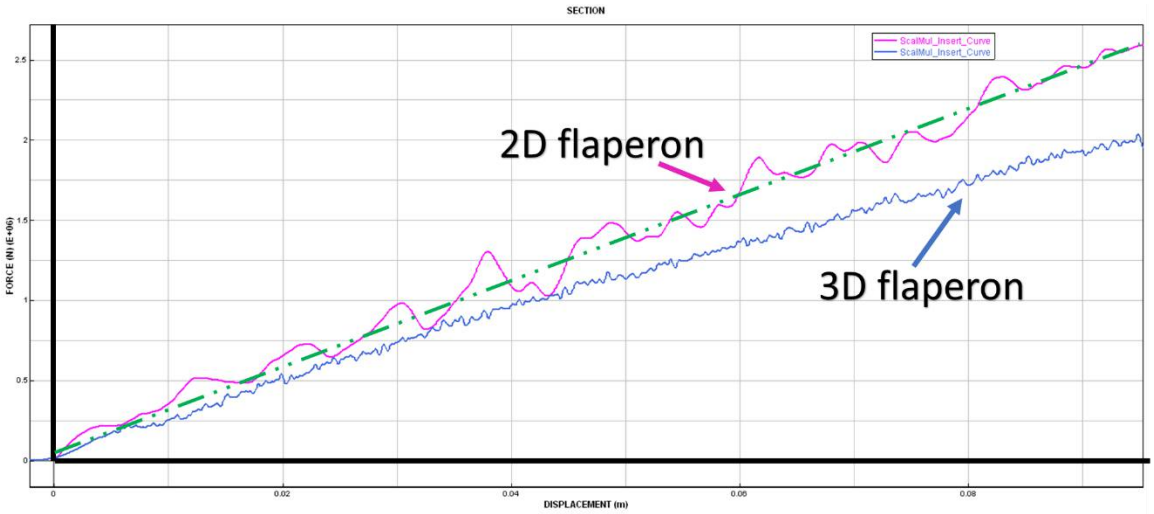

Fig. 16 SPH ditching simulation of rigid flaperon / comparison of force versus immersion depth evolution between 2D and 3D models

For the particular dimensions of the flaperon and 30 degrees inclination, the C_{3D} coefficient was found to be almost 0.75, ie.:

$$C_{3D} \sim \frac{3}{4} \tag{20}$$

and as this coefficient should depend on the Aspect Ratio AR, the flaperon has an AR almost 1, while longer structures like flaps should have C_{3D} between 0.75 and 1, hence they should tend to see higher hydrodynamic loads for the same impact configuration. In the case where the flaperon should be un-extended, it will benefit from the "confinement" of the adjacent wing components (ie. flaps) and this coefficient should be practically 1. This will be the case also if the flaperon is extended say at 30 degrees while the flaps are also extended in "landing" position, they will provide confinement and a C_{3D} close to 1.

IX. Simulation of the guided ditching of an elastic flaperon in 3D

In order to assess the potential for fracture of the flaperon around the section where the debris showed the failure happened, we need to consider simulating an elastic flaperon model that includes damage and failure.

Reference [1] was used to extract the geometric and material attributes of the flaperon. It is clearly noted that the outer skin (upper and lower) is composed from two fabric laminates separated by a honeycomb core. Each fabric laminate is composed by three fabric plies with a +/-45 , 0/90 and +/-45 degrees stackup sequence as shown in Fig. 17.

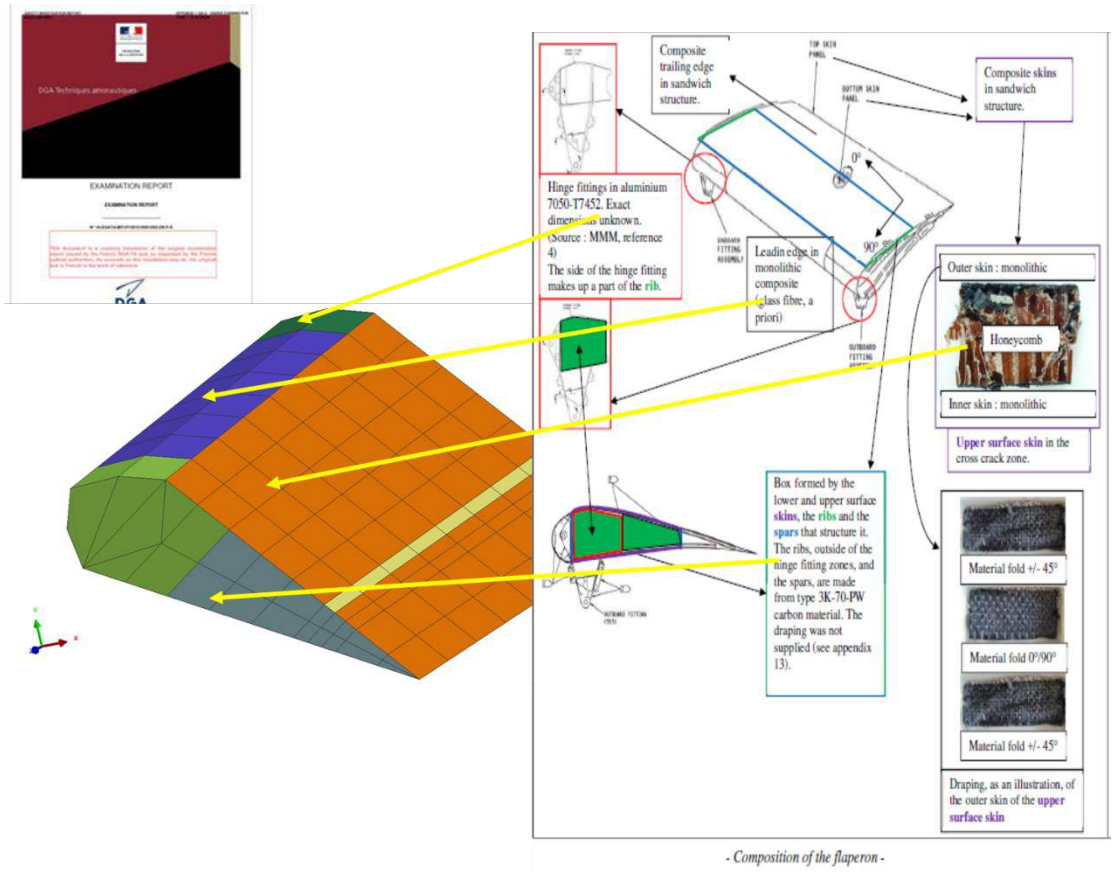

Fig. 17 Material constituents of the flaperon

The way to model such a structure was to use 3D composite material shell Finite Elements. The advanced option in the VPS code of a multi-material / multi-layered shell was used, which allows us to mix different plies with different material properties and at different orientations in the stack-up.

The details of the model creation were given in [2]. It has to be highlighted that CAPTIO did not have access to the official flaperon geometric and material description as it is property of The Boeing Company; the models were based on the limited data available in the associated DGA report of [1]. However, the ensemble of these data were reasonably representative of the essential attributes of the flaperon in order to have a convincing order of magnitude analysis of the problem in question via simulation.

The flaperon was analyzed under a guided ditching scenario with a constant 68.42 m/s horizontal speed and a constant 10.16 m/s vertical speed using the elastic with damage material representation of above. The result is shown in Fig. 18 and the failure of the trailing edge just after the trailing edge spar is evident.

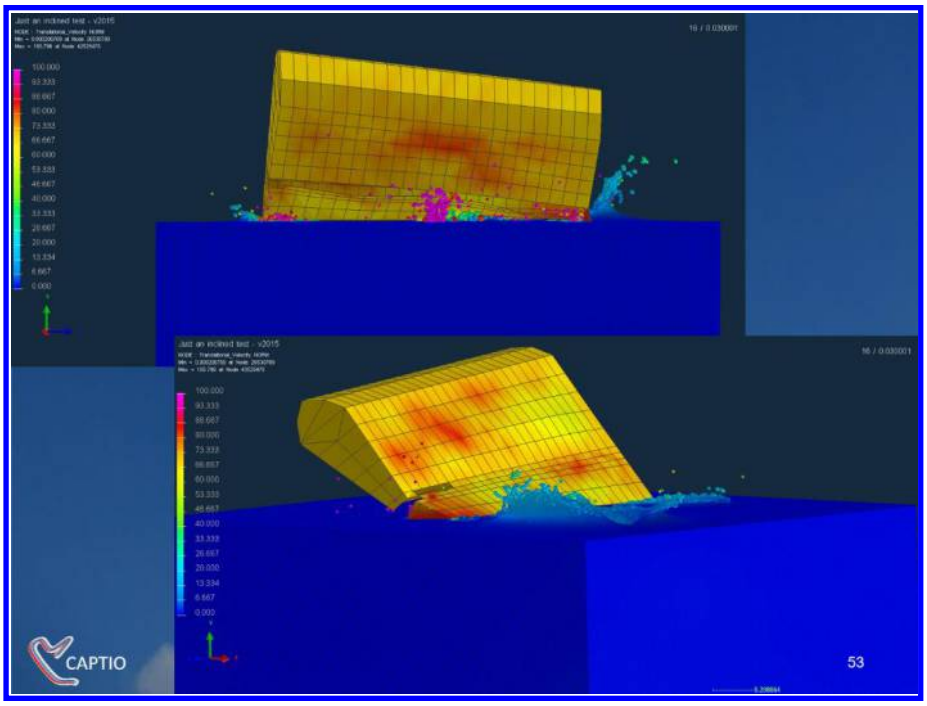

Fig. 18 Ditching simulation of the 3D elastic flaperon

This result was clearly repeatable with slight variations in material properties and also when in the extreme case an equivalent aluminum sheet ("black-aluminum") was used; a plastic hinge was always apparent behind the trailing edge spar of the flaperon.

X. Discussion of results

The comparison between the guided ditching simulation and actual recovered debris is shown in Fig. 19 below. It is obvious that it is very encouraging.

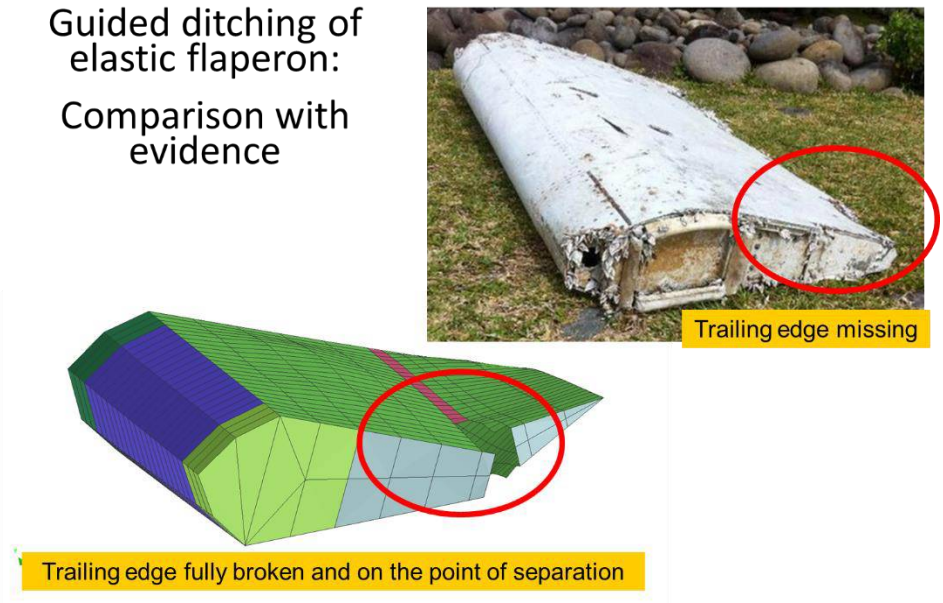

Fig. 19 Comparison of guided ditching simulations with elastic flaperon and recovered debris

The resultant vertical force variation with depth of immersion exerted upon the flaperon in the simulation was compared to the one predicted theoretically using Eq. (14) and the comparison is as below.

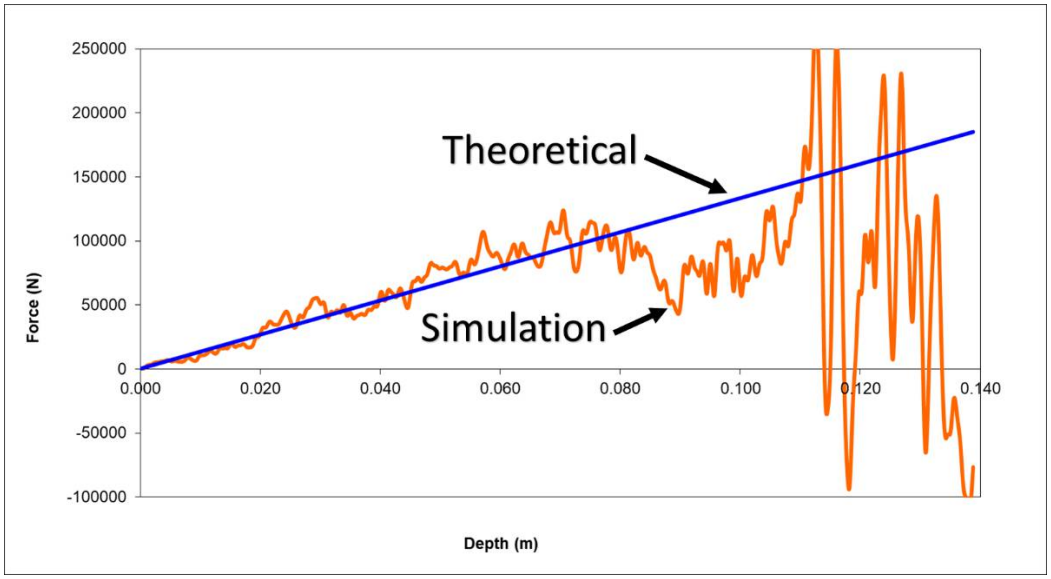

Fig. 20 Comparison of force versus immersion depth results for guided ditching simulations with elastic flaperon and theory

The comparison in Fig. 20 is evidently very good until the depth of 8cm when the damage starts to appear on the simulation model of the flaperon. The crack then propagates along the bottom skin at the intersection with the vertical spar (where the failure was observed on the debris). This translates to an erratic dynamic signal after 10 cm depth as shown above, that brings the force dynamically to zero.

In order to assess the validity of the maximum stress prediction as given by Eq. (17) around the fasteners joining the skin with the spar, the value of the maximal local average skin stress was plotted versus depth, for stress concentration factor C_σ of 2 and 3 for locally biaxial and uniaxial loadings accordingly. The corresponding curves are shown in Fig. 21.

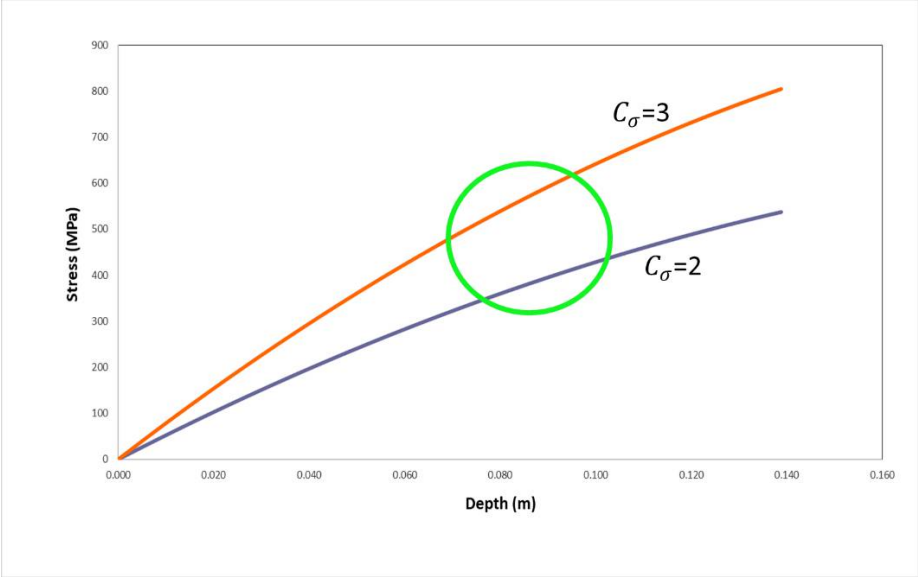

Fig. 21 Flaperon maximal local skin stress range around fastener

From Fig. 21 we can see that at depths between 8cm and 10cm and under a constant 68.42 m/s horizontal speed and a constant 10.16 m/s vertical speed, the order of magnitude of the maximal stress could be between 400 MPa and 600 MPa, which is a substantial magnitude and within fracture initiation/propagation limits for many materials.

Therefore Eq. (18) appears to be reasonably accurate in predicting when the local stress levels will be worrisome as far as fracture is concerned, for a guided ditching situation of a flaperon-like body.

Equation (18) can then be rearranged in a way to provide a relationship between horizontal and vertical speeds that can produce a certain level of maximal stress $\boldsymbol{\sigma_{max}}$ for rupture initiation (which is a material dependent constant) for a given angle α of inclination to the water free surface (which is a function of the sea state). A family of potential aircraft ditching attitude approaches can be created to be linked with other considerations like overall structural damage in order to assess the most probable "crash" scenario. This is one of the current research directions of the CAPTIO team.

XI. Conclusion

Motivated by the recovery of the MH370 Boeing 777 right wing flaperon debris and the associated suspicion that its damage was due to a ditching scenario, the author assessed the forces exerted by fluid-structure interaction upon a flaperon-like body under guided-ditching, both analytically and numerically, and compared with the evidence.

In this respect the author modified the Von Karman water impact theory by suitably redefining the added mass estimation and adapting it to a single flat panel (flaperon-like body) ditching case. He then obtained a simple analytical relation for the total hydrodynamic force as a function of horizontal and vertical speeds and angle of impact. Validation of the analytically obtained force to that obtained by Smoothed Particle Hydrodynamics (SPH) water simulations was very favorable.

The theory was further extended regarding the maximal local skin stresses of a flaperon-like body as a function of the velocity vector and angle of impact (with the perspective towards areas containing fastened parts) and a simple analytical relation was obtained. The validity of the associated formula was tested against Finite Element Model ditching simulations of the flaperon and the type and place of failure of the flaperon (notably its trailing edge) appears in accordance to the upper bounds thus obtained analytically above and towards the recovered debris.

Therefore, this simple maximum stress formula is shown to be a useful "order of magnitude" estimator of the potential for rupture of the flaperon.

The analytical work in this paper also suggests that there is an equivalence between inclined ditching and vertical immersion of a flaperon-like body with the relative speed normal to the water surface as the link. In this respect, a family of combinations of inclined ditching approaches can be created that correspond to the same overall damage potential for the flaperon and further considerations have to be taken into account in order to find the most probable one.

Acknowledgments

The author would like to acknowledge the support of the rest of the MH370-CAPTIO team, namely, Jean-Marc Garot, Jean-Luc Marchand, Michel Delarche and Philippe Gasser, who have pioneered a coherent hypothesis on the MH370 enigma. It has to be noted that the author's work, like the work of the rest of the team, is voluntary and represents only the views of MH370-CAPTIO and nobody else's.

Finally, the author, whose personal research in this paper does not involve in any way ESI Group, would like to thank ESI Group and in particular Dr Chaillou, COO, for giving him free access to ESI Group's powerful IT tools and resources.

References

[1] "APPENDIX 1.12A-2 - DEBRIS EXAMINATION, ITEM 1 – FLAPERON", *Safety Investigation Report MH370 (9M-MRO)*, Direction Générale De L'Armement (DGA), Ministère de La Défense, Sept. 2015

[2] Kamoulakos, A., Marchand, J-L., Gasser, P., Delarche, M., and Garot, J-M., "La Fin du Vol MH370 : Un Amerrissage Forcé, Étude du Flaperon Heurtant la Surface de la Mer", *LETTRE 3AF Numéro 41*, Association Aéronautique et Astronautique de France (3AF), Jan - Feb 2020. (English version available at the CAPTIO website http://mh370-captio.net/)

[3] Von Karman, T., "The Impact of Seaplane Floats During Landing", *NACA TN 321*, Oct 1929.

[4] Wagner, H., "Landing of Seaplanes", *NACA TM 622*, Jan 1931

[5] Mayo, W., L., "Analysis and Modification of Theory for Impact of Seaplanes on Water", *NACA Report No. 810*, NASA Langley Laboratory, Aug 1945

[6] Smiley, R., F., "A Semiempirical Procedure for Computing the Water Pressure Distribution on Flat and V-Bottom Prismatic Surfaces During Impact or Planing" *NACA TN 2583*, NASA Langley Laboratory, Dec 1951

[7] Szebehely, V., G., "Hydrodynamics of Slamming Ships", *Report 823*, Navy Department, July 1952
[8] Payne, P., R., "The Vertical Impact of a Wedge on a Fluid", *Ocean Engineering*, Vol 8, No. 4, pp. 421-436, Pergamon Press, 1981
[9] VPS (PAMCRASH) User's Manual, ESI Group
[10] Smiley, R., F., "An Experimental Study of Water-Pressure Distributions During Landings and Planning of a Heavily Loaded Rectangular Flat-Plate Model" *NACA TN 2453*, NASA Langley Laboratory, Sep 1951
[11] Smiley, R., F., "Water-Pressure Distributions During Landings of a Prismatic Model Having an Angle of Dead Rise of 22.5 degrees and Beam-Loading Coefficients of 0.48 and 0.97" *NACA TN 2816*, NASA Langley Laboratory, Nov 1952
[12] Smiley, R., F., "A Study of Water Pressure Distributions During Landings with Special Reference to a Prismatic Model Having a Heavy Beam Loading and a 30 degrees angle of Dead Rise" *NACA TN 2111*, NASA Langley Laboratory, Jul 1950